



**HAL**  
open science

# A sub km resolution global database of surface reflectance and emissivity based on 10-years of MODIS data

Louis Gonzalez, Francois-Marie Breon, Karine Caillault, Xavier Briottet

## ► To cite this version:

Louis Gonzalez, Francois-Marie Breon, Karine Caillault, Xavier Briottet. A sub km resolution global database of surface reflectance and emissivity based on 10-years of MODIS data. *ISPRS Journal of Photogrammetry and Remote Sensing*, 2016, 122, pp.222-235. 10.1016/j.isprsjprs.2016.10.004 . hal-01445824

**HAL Id: hal-01445824**

**<https://hal.science/hal-01445824v1>**

Submitted on 24 Jun 2021

**HAL** is a multi-disciplinary open access archive for the deposit and dissemination of scientific research documents, whether they are published or not. The documents may come from teaching and research institutions in France or abroad, or from public or private research centers.

L'archive ouverte pluridisciplinaire **HAL**, est destinée au dépôt et à la diffusion de documents scientifiques de niveau recherche, publiés ou non, émanant des établissements d'enseignement et de recherche français ou étrangers, des laboratoires publics ou privés.

# A sub km resolution global database of surface reflectance and emissivity based on 10-years of MODIS data

Louis Gonzalez<sup>1</sup>, François-Marie Bréon<sup>2</sup>, Karine Caillault, Xavier Briottet\*<sup>3</sup>

<sup>1</sup> LOA, CNRS UMR 8518, Université Lille1, Sciences et Technologies, F-59655 Villeneuve d'Ascq CEDEX, France (Louis.Gonzalez@univ-lille1.fr)

<sup>2</sup> Laboratoire des Sciences du Climat et de l'Environnement, UMR CEA-CNRS-UVSQ, F-91191 Gif-Sur-Yvette, France (Francois-Marie.breon@lscce.ipsl.fr)

<sup>3</sup> ONERA/DOTA, 2 Avenue E. Belin, BP 74025, F-31055 Toulouse, France (Karine.Caillault@onera.fr, Xavier.Briottet@onera.fr)

## Abstract

The MODIS instruments have been flying onboard the Terra and Aqua platforms and have acquired Earth observation data since early 2000 and mid 2002, respectively. After atmospheric correction, the collected data allows the monitoring of the land cover dynamics. Here, we describe a data processing scheme to generate Earth reflectance and emissivity time series at a sub-kilometer spatial resolution and with a period of 8 days. The data processing scheme removes residual cloud and aerosol contamination in the MODIS products, applies directional correction, and fills the gaps resulting from persistent cloud cover. The resulting database, referred to FondsDeSol, offers a significant improvement with respect to the first version proposed in (Gonzalez et al., 2010), and covers a period of ten years against only one year for the first version. The first motivation of the database is to improve the estimation of at sensor radiances for the design of future sensor in the optical domain. Nevertheless, such database opens the way to new research topics like land surface dynamics, land cover changes, and inter-annual variations due to climate perturbations.

**Keywords:** Reflectance; MODIS; TERRA; AQUA; climatology; global database; 500 meters; 8 days; 10 years;

## 1 Introduction

In the optical domain, worldwide spectral surface reflectance climatology is necessary to design any future space borne missions by providing technical characteristics like observable radiances, signal noise ratios, etc. The design of new sensors is achieved from surface reflectances acquired by the targeted sensor using an end-to-end simulator. The latter is able to model first the signal incident to the sensor, second the output signal taking into account its main imaging system characteristics and its related preprocessing, and finally estimates the retrieved signal on ground surface properties after an atmospheric compensation processing. Several end-to-end simulators already exist such as SENSOR (Börner et al., 2001) developed for the preparation of the Airborne Prism Experiment (APEX) (Itten et al., 1997), the simulators to specify the SPECTRA mission (Verhoef et al., 2003), Pléiades to sense urban area (Miesch et al., 2004) or the future Sysiphe (Rousset-Rouvière et al., 2011) hyperspectral airborne mission, the Parameterized Image Chain Analysis & Simulation Software (PICASSO) (Cota et al., 2010), the tool to prepare the Compact Reconnaissance Imaging Spectrometer for Mars (CRISM) (Parente et al., 2010), or the EnMap simulator (Segl et al., 2012). All of these end-to-end simulation tools are implemented in a modular and flexible way so that they can be applied to a large variety of sensors and environmental parameters. Nevertheless, one key point to achieve realistic simulations in a statistical sense is to provide to the simulator representative inputs like ground spectral emissivity and reflectance. The availability of such optical properties is not direct and presents some limitations depending on the measurement conditions: on ground, airborne or space borne.

Ground optical properties usually come from existing database built from laboratory measurements. LOPEX'93 (Leaf Optical Properties EXperiment) (Hosgood et al., 1995) carried out by the European Commission Joint Research Center collected spectral measurements of various elements (leaf, pine needle, stalk, ...) of several vegetation types in the spectral band (0.4-2.5  $\mu\text{m}$ ). ASTER (Advanced Spectral Emission and Reflection Radiometer) database (Baldrige et al., 2009) includes a large variety of natural and artificial material spectra (0.4-14  $\mu\text{m}$ ) and pure minerals. Even if such data sets are covering a wide range of materials, a first drawback is that these optical properties are measured with a typical sample size on the order of a few cm, which is not representative of spaceborne sensor GSD (Ground Sampling Distance). Secondly, such databases do not consider the temporal variability of these properties in a given geographic location. Combining these spectra with a global land cover database offers the possibility to build a global coverage in optical properties but with neither temporal nor climatological representativeness. By making

full use of the huge amount of remote sensing data, it is possible to overcome such limitations, with the aim of creating a worldwide climatology of surface optical properties. A first climatology has been proposed by Meygret et al. (1997), in the BDHS (Base de Données Histogramme Spot), but it only delivers the top of atmosphere (TOA) reflectances in the 4 Spot bands. More recently with the advent of new multispectral sensors like VEGETATION (Bartholomé, & Belward, 2005), MERIS (Arino et al., 2008), and Bontemps et al., 2010), MODIS (Friedl et al., 2002, 2010), numerous works have been presented to build surface reflectance databases. For example, GlobCover (Arino et al., 2008, Bicheron et al., 2008) which is based on 1-year MERIS measurements, gives 15-days products with a 300-meter spatial resolution in the Visible band; GlobAlbedo data of the land surface (Muller et al., 2011, 2012) are being produced from European satellites data from 1998 - 2011 with a spatial resolution of 1 km, between 0.3 and 3  $\mu\text{m}$  (<http://www.GlobAlbedo.org>); ADAM (A surface reflectance DATABASE for ESA's earth observation Missions) is a global monthly reflectance climatology (ADAM-ESA) constructed from MODIS measurements on a  $0.1^\circ \times 0.1^\circ$  grid over the 0.3-4  $\mu\text{m}$  spectral range (<http://adam.noveltis.com>). Nevertheless, these databases suffer from one or several limitations: 1) the temporal resolution: they mainly deliver monthly products, except the GlobCover products (15 days); 2) the spectral coverage is restricted to visible and near infrared bands; 3) most of these processed data sets are temporally limited to 1 to 2 years. It appears thus crucial to simultaneously improve the spatial and temporal resolutions but also the spectral extension of reflectance databases for an optimal specification of future space missions like HYPXIM (Carrere et al., 2014) or MISTIGRI (Lagouarde et al., 2013).

To go beyond existing databases, one can fully exploit the two MODIS sensors onboard Terra and Aqua platforms, which since 1999 (Terra) and 2002 (Aqua) continuously acquire images of the Earth at a resolution between 250 m and 1 km, depending on the spectral bands covering visible, solar infrared and thermal infrared spectral regions. In this work, we focus on the monitoring of land surfaces dynamics by building a database over 10 years (2003—2012) with high a temporal sampling resolution. The difficulties encountered in the processing of MODIS data have various origins: 1) the MODIS products are not free from artifacts, such as unscreened atmospheric influence or other unwanted effects; 2) the input reflectance time-series cannot be directly exploited and interpreted because of their large time variability that results from the anisotropic properties of land surface reflectances. This paper presents a robust and reliable processing of MODIS data set leading to a reflectance database called FondsDeSol (FDS) that, in a very-near future, will be disseminated through an easy-to-use web interface ([http://newtec.univ-lille1.fr/fondsdesol/index\\_ch.html](http://newtec.univ-lille1.fr/fondsdesol/index_ch.html)). FDS is built with a frequency of 8 days, re-projected on a “plate-carrée” grid ( $\pm 85^\circ/\pm 180^\circ$ ) and contains the spectral reflectance (respectively emissivity) of all MODIS wavelengths at a resolution of 500 m (resp. 1 km). Original data is cleaned from all pixel artifacts. Moreover, ground reflectances are corrected from bi-directionality effects and normalized to a fixed sun and viewing geometry. Therefore, the database can be used either to retrieve directional surface reflectances and albedos or to compute spherical albedos.

Section 2 describes the data processing algorithm, which identifies corrupted measurements, normalizes the directional effects of valid observation, and gap-fills the reflectance time series. Section 3 provides a comparison of the resulting database to the standard MODIS product, to an earlier version of FondsDeSol (Gonzalez et al., 2010), and to the reflectance MCD43C4 product. The temporal resolution of FondsDeSol is highlighted by examples of specific events that have been identified and analyzed. Finally, conclusions are given in section 4.

## 2 Algorithm description

### 2.1 Input data

The main input data of the processing chain is the NASA MOD09A1 product, which is available from the two MODIS instruments on board the TERRA and AQUA satellites. The product provides the surface reflectance, after atmospheric correction, in 7 spectral bands ranging from 459 nm to 2155 nm on a sinusoidal projection grid at a 500m GSD. The best observation over the 8 days period is kept, based on criteria on cloud and aerosol contaminations. The MOD09A1 product also includes the day and the observation geometry of the selected measurement. In addition, we also use two other NASA products over the same time period: the MOD11A2 product, which provides an estimate of the land surface temperature and emissivity derived from MODIS data over global land surfaces under clear-sky conditions; and the MOD10A2 product which quantifies the snow/ice land cover.

The directional signature correction, described below, requires the knowledge of the surface type, which is known at the pixel level through the global land cover classification provided by the MOD12Q1 product. This set of cover types (IGBP) includes eleven categories of natural vegetation covers; three classes of developed and mosaic lands, and three classes of non-vegetated lands. One improvement of FondsDeSol with respect to the 2006 version, is the discrimination of snowy pixels using the snow cover product (MOD10A2) that includes the maximum snow cover extent and a snow occurrence observation over an 8-day period that can be compared to the MOD09 internal snow flag.

## 2.2 Algorithm principle

Although the MOD09 processing aims at the identification of cloud or snow contamination and corrects for aerosol scattering, the analysis of reflectance images and time series clearly indicates the presence of remaining contamination. In addition, the measured reflectances have not been corrected from directional effects, which impact the time series. Finally, persistent cloud cover sometimes prevents any observation during the 8-day synthesis period, which leaves gaps in the time series. The data processing, described below, aims at mitigating these defaults. Altogether, the designed algorithm provides reasonable reflectance values, which in practice corresponds to either the true reflectance, or to a realistic value whenever the contaminated pixels dominate.

A 4-steps algorithm is proposed with the objective to keep the general dynamic of the original measurements, to reject the contaminated measurements, and to rebuild the incomplete time series as close as possible to reality. These 4 steps are:

1. Apply a bidirectional reflectance distribution function (BRDF) correction to normalize reflectances.
2. Filter the strongly contaminated pixels from clouds and clouds shadows based on a contrast method and compute the mean values over 4 consecutive 8-days periods for both satellites (hereafter referred to as time window). This average is recomputed with a time-shift of 8-days, leading to a moving average with a weekly time-resolution.
3. Fill the missing data through either a simple temporal interpolation or by using data from a nearby pixel having a similar multi-spectral signature and land classification.
4. Final generation and projection.

## 2.3 Step 1: Bidirectional Signature Corrections

Land surface reflectances vary by a factor of more than two as a function of the observation geometry. For quantitative use of the reflectance time series, it is therefore essential to normalize the measurements to a given observation geometry. In the following, we define this reference geometry as (solar zenithal angle  $\theta_s = 40^\circ$ , and satellite zenithal angle  $\theta_v = 0$ ). For all other pixels, we apply a BRDF correction that depends on both the type of land cover and the observation geometry (sun, satellite). The land cover type is defined from the IGBP product where 17 ones are proposed. Thus, the corresponding BRDF correction is defined as follows:

$$\rho(40^\circ, 0^\circ, 0^\circ)^* = \rho(\theta_s, \theta_v, \Phi) \cdot \frac{BRDF(40^\circ, 0^\circ, 0^\circ)}{BRDF(\theta_s, \theta_v, \Phi)}$$

where  $\rho(\theta_s, \theta_v, \Phi)$  represents a MODIS acquisition in a given band in the viewing conditions defined by the solar zenithal angle ( $\theta_s$ ), the view zenithal angle ( $\theta_v$ ) and the difference between the solar and viewing azimuth angles ( $\Phi$ ).  $BRDF(\theta_s, \theta_v, \Phi)$  is the BRDF model attached to a given land cover type.

For most of the land cover type, the « *Ross-Li Hot Spot* » model is used (Maignan et al., 2004a, 2004b, Bacour et al., 2008)

$$BRDF(\theta_s, \theta_v, \Phi)^* = k_0 \left[ 1 + \frac{k_1}{k_0} \cdot F_1(\theta_s, \theta_v, \Phi) + \frac{k_2}{k_0} \cdot F_2(\theta_s, \theta_v, \Phi) \right]$$

For a given biome, its corresponding parameters ( $k_0$ ,  $k_1$ ,  $k_2$ ) are estimated from POLDER and PARASOL measurements over several soil types defined by their normalized difference vegetation index (NDVI). Four intervals of NDVI are considered: [-0.2, 0.2], [0.2, 0.5], [0.5, 0.8], [0.8, 1.0].

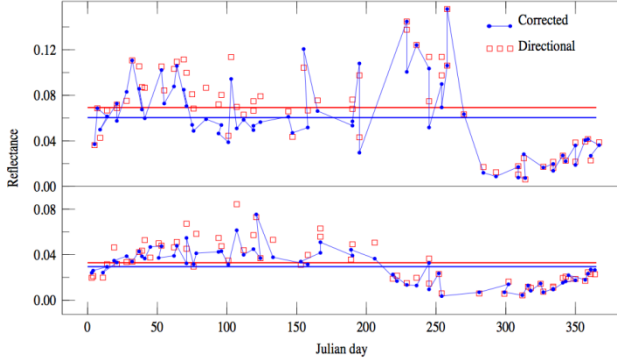
Over barren or sparsely vegetated areas (bright areas in Fig. 1), reflectance values turn out to be underestimated. The error evaluation was done by looking at the difference between AQUA and TERRA reflectances before and after correction (a perfect correction must give close values for both measurements). The initial Ross-Li coefficients,  $k_0$ ,  $a$ , and  $b$  are readjusted by an iterative algorithm fitted using the measured

reflectance:

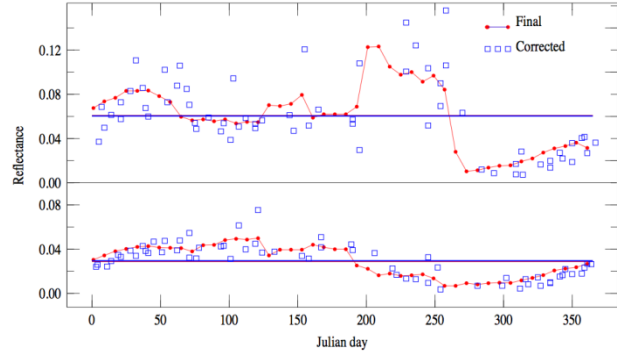
$$\frac{k_2}{k_0} = a_\lambda \cdot k_{0,\lambda_{typic}} + b_\lambda$$

with the initial value  $k_0 = \frac{\rho_{ref\,measure}}{1 + C \cdot F_1 + \frac{k_2}{k_0} \cdot F_2}$ , C being a constant.

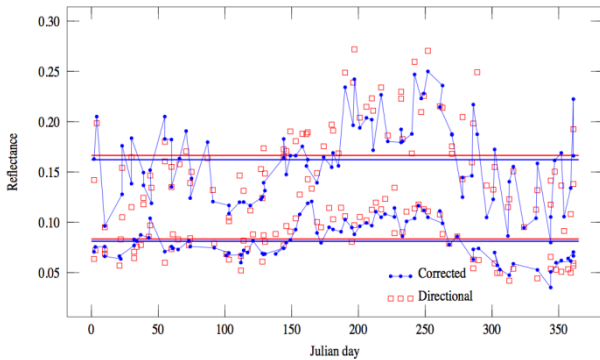
### Mixed Forests



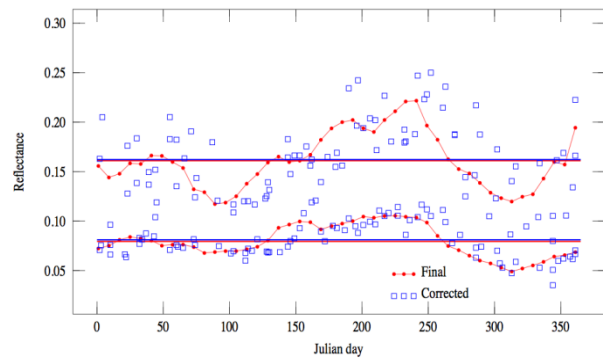
### Mixed Forests



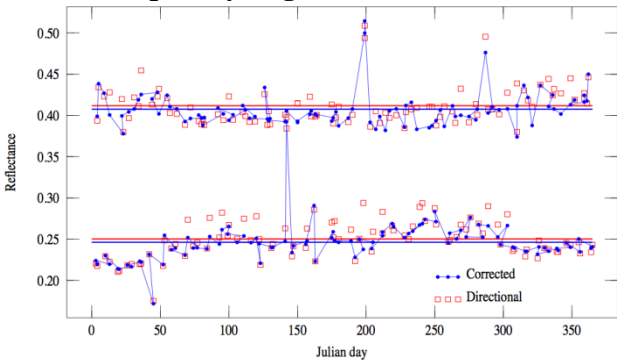
### Savannahs/Grasslands



### Savannahs/Grasslands



### Barren or Sparsely Vegetated



### Barren or Sparsely Vegetated

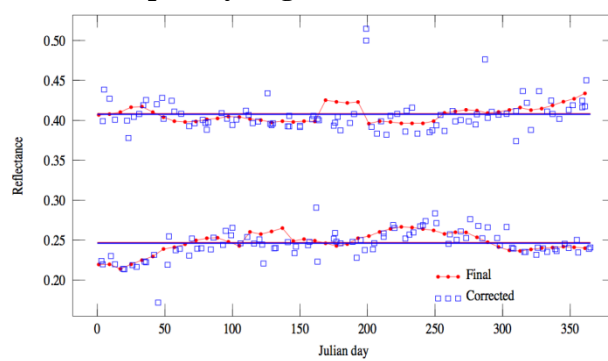


**Fig. 1** Impact of the directional correction and the moving-average smoothing, to reduce the natural noise of the input measures on different types of landscape: barren from Sahara, Savannahs and grassland in the north of Spain and mixed forest from Cambodia. For each case, a brighter (top curve) and a darker area (lowest curve) are selected to point out directional effects. The left graphics show in red the input data with the directionality effects and in blue the BRDF corrected signals. The right graphics show the BRDF corrected signals (blue dots) and the final results in red after a 4-period window filtering.

Generally, the algorithm converges after two or three iterations. Examples of the initial parameters computed from POLDER/PARASOL measurements for three particular wavelengths:  $\lambda = 565 \text{ nm}$ ,  $670 \text{ nm}$ ,  $865 \text{ nm}$  are listed in Table 1. Snow-covered pixels are treated with a specific reflectance model of Kokhanovsky et al., (2012). Fig. 1 (left) shows reflectance time series of the MOD09A1 product, before and after BRDF corrections, revealing the magnitude of bidirectional effects. Fig. 1 (right) illustrates how the moving average eliminates high temporal variations, but keeps the general seasonal behavior.

**Table 1.** Initial parameters for the Ross-Li model presented in Section 2.3.

| $\lambda$ (nm) | $k_0$ ref | c       | a       | b      |
|----------------|-----------|---------|---------|--------|
| 565            | 0.2611    | -0.0093 | -1.9138 | 1.5973 |
| 670            | 0.3816    | 0.0144  | -2.0520 | 1.4097 |
| 865            | 0.4746    | 0.0353  | -1.9469 | 1.3208 |

## 2.4 Step 2: Identification of contaminated measurements and smoothing

The moving average is then computed every 8-days. Each average is composed of data acquired over 4 successive 8-days periods rejecting various types of anomalies. The maximum of available measurements is 8 (4 per satellite). The identification of contaminated measurements and smoothing is performed in two steps:

- 1) Rejection of pixels affected by either clouds or bad sensor scans (see section 2.4.1)
- 2) In the case of the number of remaining pixels over 4 8-days periods is more than 5, a moving average is achieved to smoothen short-time frame variations (see section 2.4.2). In other cases, such as very cloudy areas, good measurements have to be fetched as described in section 2.5.

### 2.4.1 Artifact detection and pixel list building

To discriminate erroneous pixels from “good” ones, a spectral contrast test has been developed, named “pixel contrast ratio” PCR. It is defined as the standard deviation of the spectral reflectance in the three visible bands (0.459, 0.545, 0.620  $\mu\text{m}$ ), divided by the mean reflectance over the same channels:

$$PCR = \frac{1}{x_\lambda} \sqrt{\sum_{i=1}^3 (x_{\lambda_i} - \bar{x}_\lambda)^2}$$

where  $x_{\lambda_i}$  is the measured reflectance in band  $i$ .

Cloud, aerosols, or snow contamination tends to lower the spectral contrast. A pixel is identified as being contaminated if the contrast  $P$  is smaller than a threshold  $T_{\text{cloud\_or\_shadow}}$  that is nominally set to 0.04. This empirical threshold was determined through the analysis of several mid latitudes and equatorial geographic areas, and by steadily increasing its value until the extinction of all bad pixels was satisfactory. However, if the quoted threshold rejects too many points (more than 3 out of 8) in our time-window, the data set is explored in the adjacent  $\pm 3$  years with the same time window as illustrated by the scheme displayed on **Fig. 2**; the process ends when five points are selected. If the adjacent search is unsuccessful, the threshold value is reduced until a representative number of pixels to compute the mean  $P$  can be found. This adjustment is necessary over very bright areas or very dark natural scenes. If the selection threshold has to be reduced, the corresponding pixel is flagged as “suspicious”. However, if a pixel is traced “suspicious” over a long time, it might in fact correspond to a naturally very dark or very bright area. The pixel will thus be untagged in the times series analysis. If the searching process completely failed, the pixel is flagged as “cloudy”. **Fig. 3** displays a true color composite and highlights areas where the PCR tests improve the quality of the filtering process, before the moving average is computed.

## Pixel Construction

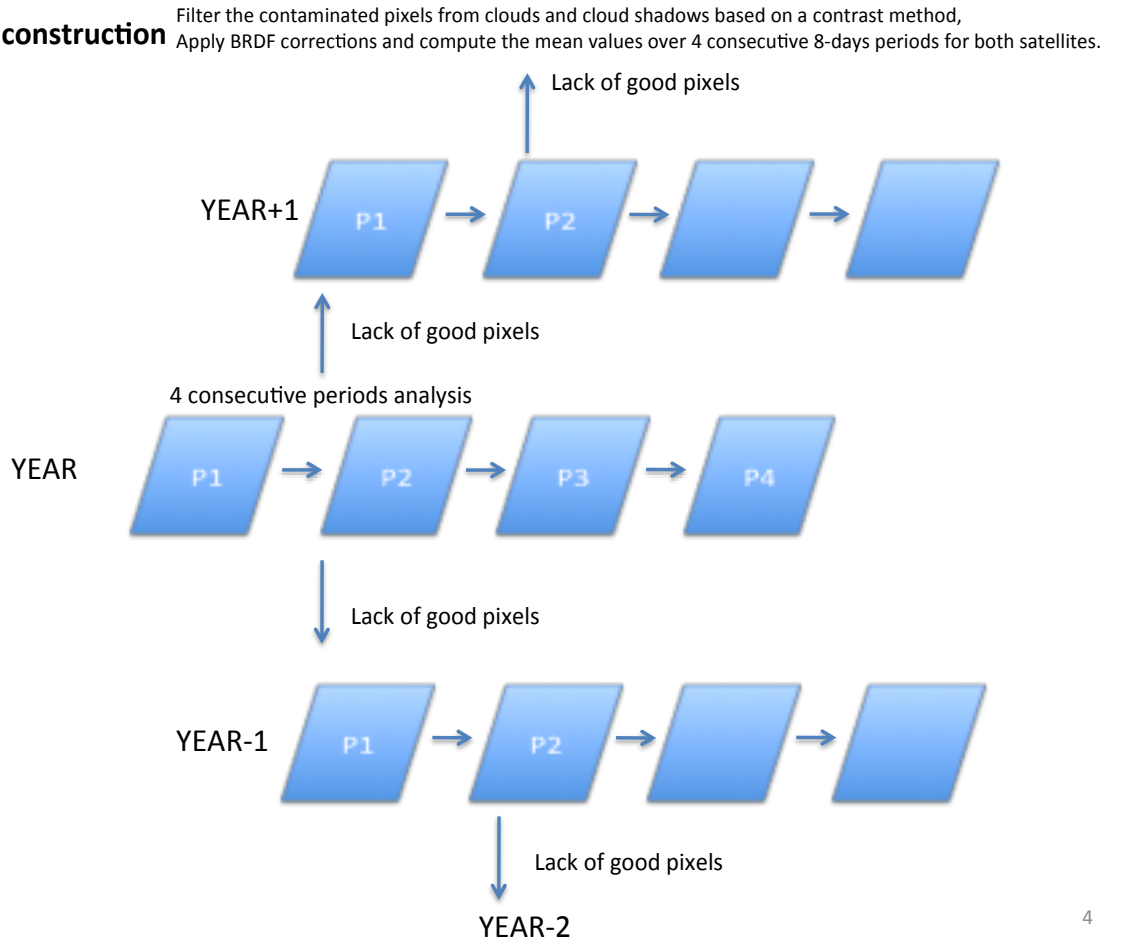


**Fig. 2** Flowchart of the Pixel Contrast ratio (PCR). The maximum number of observations is 8; if it is less than 5 points, new pixels are added from the same location using adjacent time-windows over several years (first year  $\pm 1$  then year  $\pm 2$ , etc..) to obtain 5 or more pixels (The interval  $\pm 3$  years was good enough to find pixels).



**Fig. 3** Left: image of true color composite in reflectances acquired in Nigeria (-9.53W, -6.063E, 8.53N, 6.15S) on the 17<sup>th</sup> of January, the reflectances are derived from a composite of 4 MOD09 periods. The magenta pixels represent the ones rejected as definitely cloudy, the orange color correspond to areas where the PCR test rejects at least one data among the 8 input values (scratch from bad inputs are clearly detected). Right: the yellow color reveals the areas where less than 5 pixels are used to compute the mean reflectance result.

### 2.4.2 Time-window smoothing algorithm

In most areas, the PCR selects a minimum of 5 data points. However, for very cloudy areas, clouds may still spoil some of these values. To remove these anomalous points, we further filter the data, by rejecting all points that deviate by more than 40% (this selection threshold was chosen empirically over very cloudy areas) from the median value, and perform the final average for a given band  $\lambda_i$ ,  $\rho(40^\circ, 0^\circ, 0^\circ)_{\lambda_i t}$ , over the M number of remaining pixels.

This processing is repeated all year long with a shift of one 8-days period. The use of a 4-weeks moving average helps monitoring realistic reflectance time-evolutions, by filtering out the “noise” arising from short-term spurious fluctuations, such as remaining clouds or smokes. The right side of Fig. 1 highlights in red the final result of temporal smoothing, which effectively integrates the data from the two MODIS satellites. This figure illustrates how the noise is filtered and how the short, medium and longer-term trends are preserved, to build seamless reflectance profiles.

### 2.5 Step 3: Patching the “suspicious” pixels in the time series

By monitoring during one year (46 8-days periods) the variations of the reflectance at each pixel, the cloudy and “suspicious” areas in the images are either rebuilt or kept or rejected. Empirically the times series are classified into three main families, each corresponding to a different correction protocol:

- **Ideal time series:** alternating “cloudy”/”suspicious” and clean pixels. The reflectance reconstruction is carried out by interpolating the missing cloudy values from the cloud-free ones close in time. If the temporal gap between two clean observations is larger than 3 time-periods, we use the “very cloudy time series” protocol.
- **Very cloudy time series.** In the absence of reflectance values, we first try to substitute the missing data with the values of the neighboring years, and second with values of pixels having similar biome and spatially close (See Fig. 4).
- **Time series with constant indetermination over ten years.** Such cases have been found in very bright areas such as salt lakes. The corresponding “suspicious” flags are cleared and the reflectance values are estimated in the same way as for ideal time series.

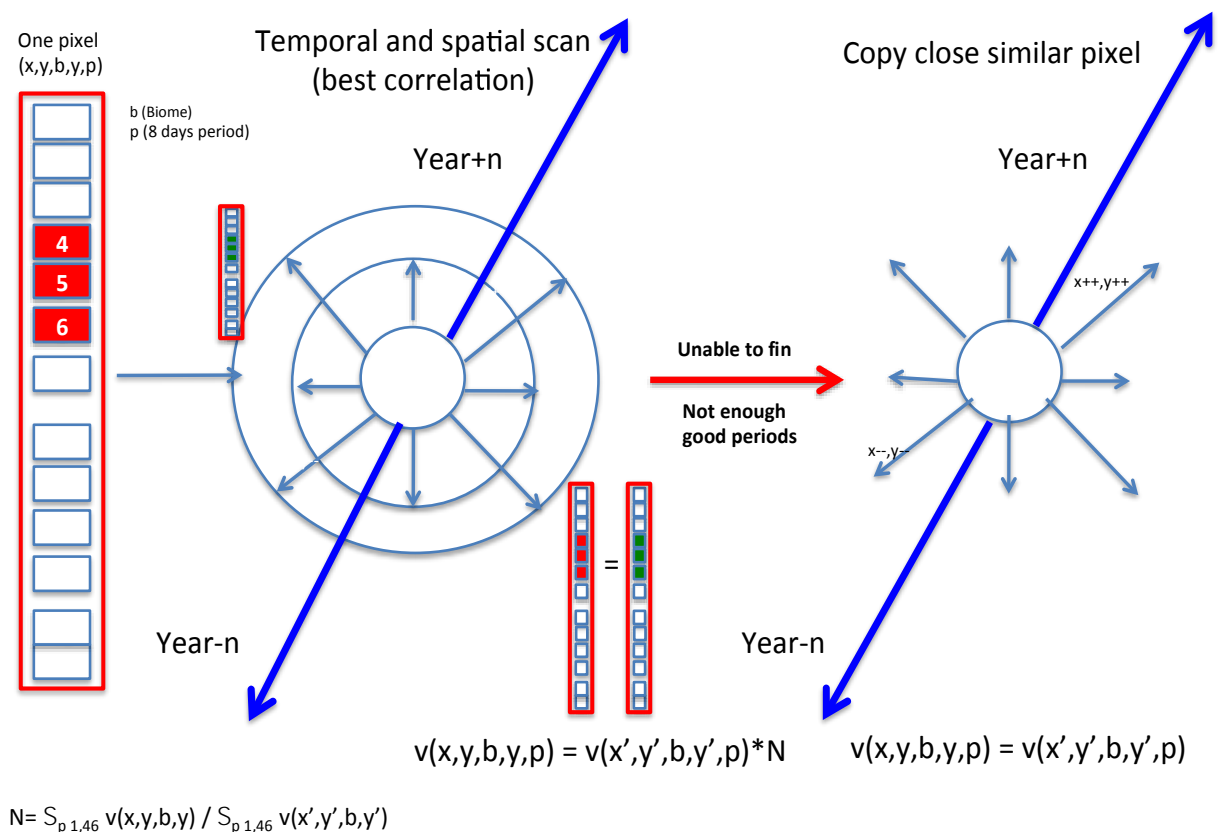


**Fig. 4** Principle of the “suspicious” pixels processing in times series. In red are the missing values in a one-year series (46 8-days periods); in order to fill the gaps the database is explored to look for a similar biome close in distance and time. The missing values are then picked up from the similar biome and normalized by the ratio of the averaged signal of the two biomes.

Fig. 5 shows the percentage of pixels for which the reconstruction requires data points from neighboring years for year 2006. It appears that the spatial distribution is well correlated to either the cloud coverage or the snow coverage of the geographical areas.

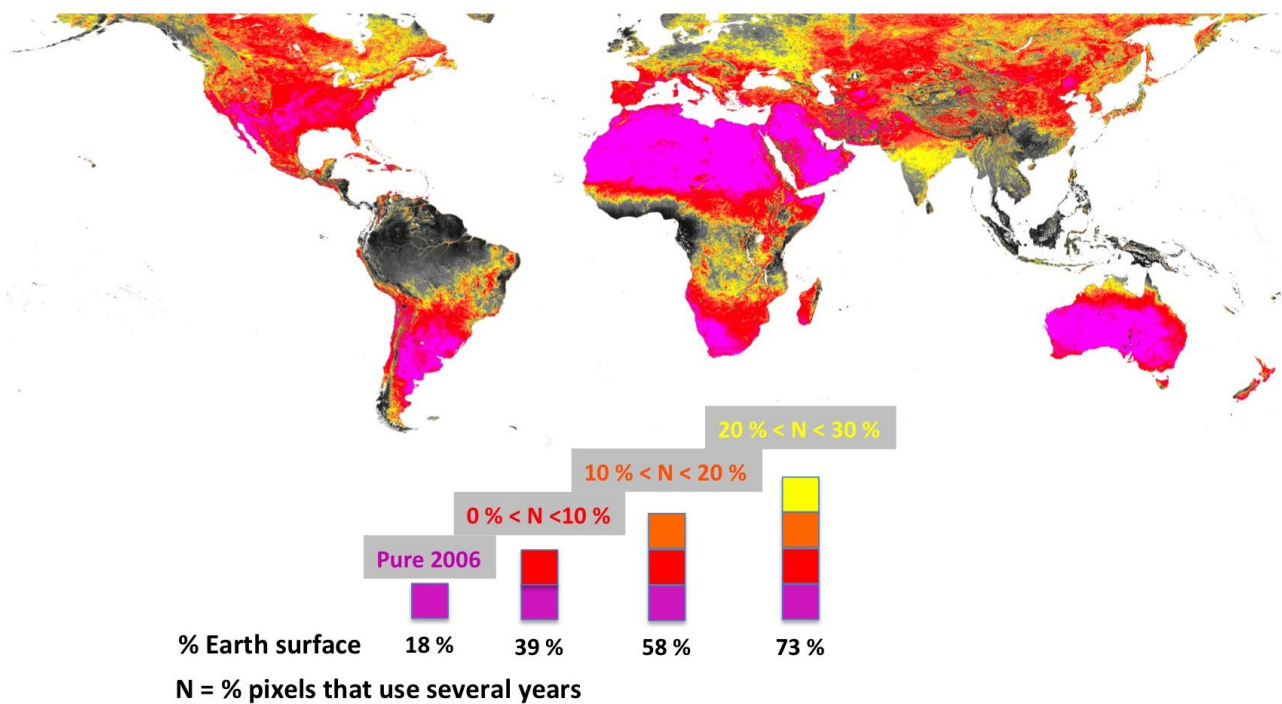


**Fig. 5** Global impact map of the multi-year pixel reconstruction for the 46 periods of 2006. The color legend represents the percentage of pixels that uses more than one year of input data, and the corresponding percentage of the Earth surface. Grey areas have more than 30 % of multi-year reconstructed pixels (the darker the grey, the higher the number of years involved).

## 2.6 Step 4: Final generation and projection

The final results are dumped as 46 slots per year projected on a 500 m plate-carrée grid in an HDF4 compressed format. In addition to reflectance, MODIS emissivities and land surface temperatures are time-averaged and remapped from the original 1 km resolution to the final 500m grid by near pixel interpolation. Auxiliary data, such as biome types and vegetation indexes are also included to enable retrievals of reflectance in any geometry.

## 3 Quality of the new FondsDeSol database

### 3.1 Improvements with respect to the first version generated in 2007

The first version (V0) was using one year (2006) of MOD09A1 data collection 4, the new version (V1) integrates 10 years of MOD09A1 collection 5. The quality of the V1 release benefits from the selection of good pixels using, if necessary, data from adjacent equivalent biomes in distance and time (See Section 2.5). Another improvement over V0 is the use of MOD10A2 snow detection that replaces in V1 the internal MOD09A1 snow flag.

To demonstrate the efficiency of the new algorithm with respect to cloud/snow filtering we have selected several illustrative areas. Fig. 6 displays a visible-band composite (0.620, 0.545, 0.459  $\mu\text{m}$  channels as RGB) showing clearly the impact of the new reconstruction over a very cloudy region of Indonesia. Fig. 7 and Fig. 8 compare reflectance values of the two FondsDeSol versions over transects in desert and deep forest areas. As expected, V0 and V1 are very close in the deserts, while V1 values are smaller than V0 in the very cloudy regions such as deep forests as a result of the better cloud screening. The global map of the absolute relative errors  $((V1-V0)/V1)$  between V0 and V1 versions (Fig. 9a) reveals that the largest changes correspond to the

cloudiest areas. In snowy regions, northern Earth regions in wintertime, Fig. 9b illustrates the significant impact of the MODIS snow product on the reconstructed reflectance.

### Final result: Impact over very cloudy regions

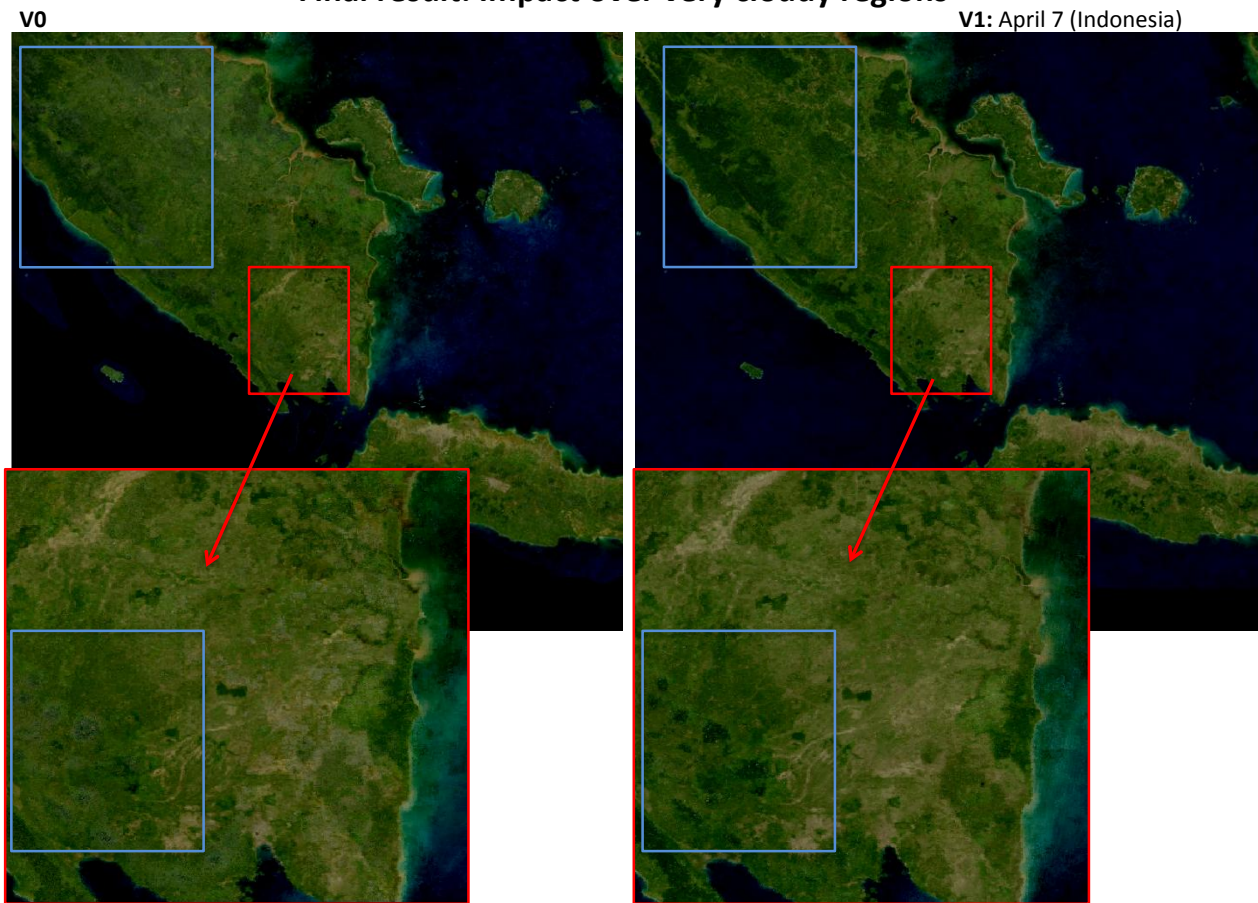


**Fig. 6** Impact of the reconstruction in a very cloudy region of Indonesia; it illustrates that the canopy is less noisy in V1 (right) than in V0 (left).

## Overdesert

Reflectances  $\lambda$  620  $\mu\text{m}$   $V1/V0$  1.98

545  $\mu\text{m}$  1.97

459  $\mu\text{m}$  1.94

?

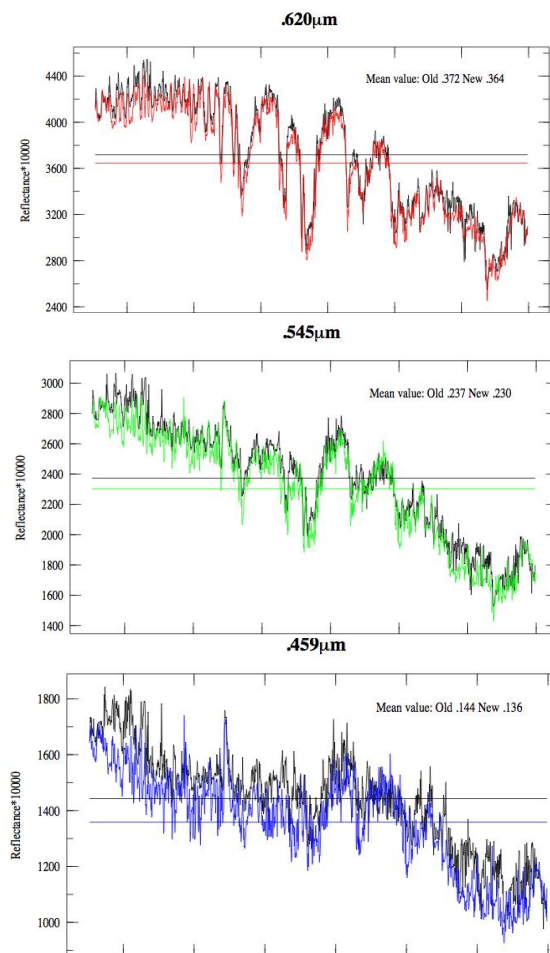


**Fig. 7** Impact of our reconstruction method in the desert. The right hand side graphs reveal the close similarity between the reflectance values computed across the magenta transect for the red, green and blue visible bands, as computed by V1 (colored lines) and V0 (black lines). The quoted V1/V0 values are the ratios between the mean values of the two FDS versions. The horizontal lines represent the mean values of each data sets.

**Over deep forest**

Reflectances at 620nm V1/V0 = 1.76  
 at 545nm V1/V0 = 1.85  
 at 459nm V1/V0 = 1.76

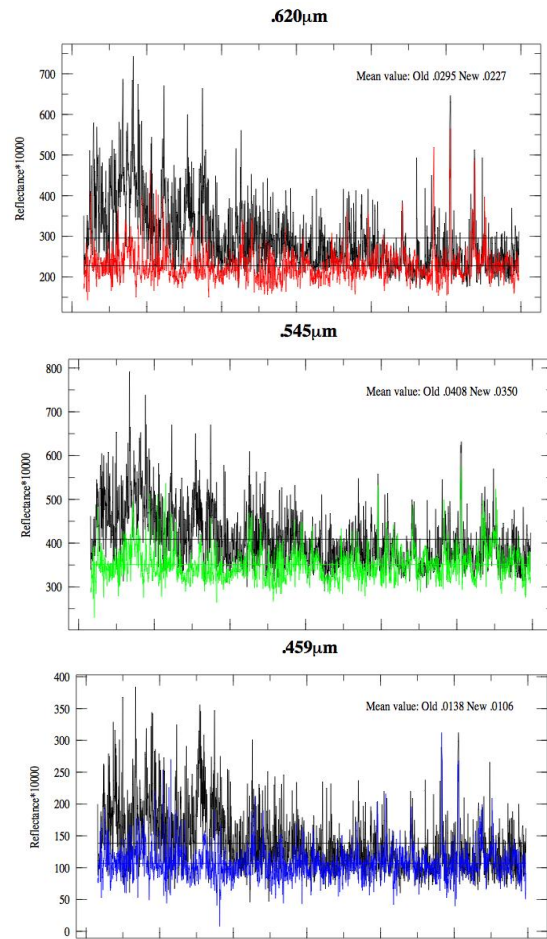
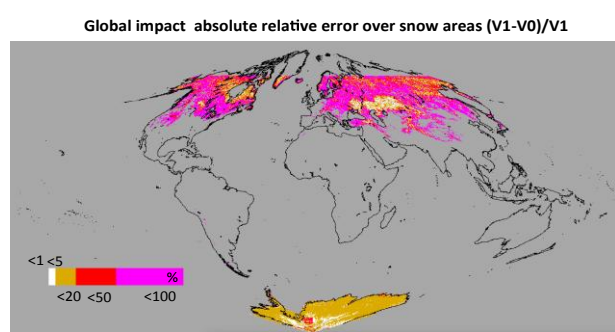
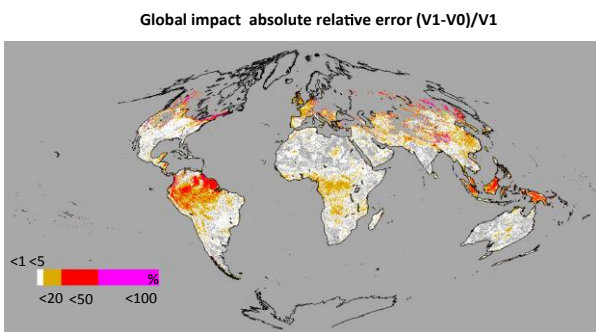


**Fig. 8** Impact of our reconstruction method over deep forest. The right hand side graphs display the reflectance values computed across the magenta transect for the red, green and blue visible bands, as computed by V1 (colored lines) and V0 (black lines), highlighting the improvements brought by the V1 FondsDeSol algorithm. The quoted V1/V0 values are the ratios between the mean values of the two FDS versions. The horizontal lines represent the mean values of each data sets.



(a)

(b)

**Fig. 9** Absolute relative errors between V0 and V1 FDS versions ((V1-V0)/V1) over land (a) and snow (b) areas.

### 3.2 Comparison with the MCD43C4 Reflectance product (2006)

To evaluate the quality of FDS V1, our results are compared to the (MODIS) Reflectance product (MCD43C4), using the collection 5 of the dataset downloaded from (<http://e4ftl01.cr.usgs.gov/MOTA/MCD43C4.005>) (the same collection level was used to build FDS). The product is delivered with a resolution of  $0.05^\circ$  (5.6 km). We have selected only the best quality pixels according to the quality index of the MCD product. Here, we focused our evaluation on the three visible bands (0.620, 0.545, 0.459  $\mu\text{m}$ ) and build for both data sets a year mean reflectance at the same resolution and geometry ( $\theta_s$ =local solar noon,  $\theta_v$ =0). FDS and MCD records were synchronized: we select only the FDS pixels whenever they exist in MCD, implying that the final annual mean results have empty areas (there is missing data all year long in the MCD product at the best quality pixels index)

**Fig. 10** compares the reflectance values computed from MCD and FDS along a large transect over the Sahara. As expected the correlations and standard deviations between both data sets are excellent for the red, green and blue bands respectively with: correlation coefficient of 0.99, 0.99 and 0.98, and standard deviations less than 0.008.

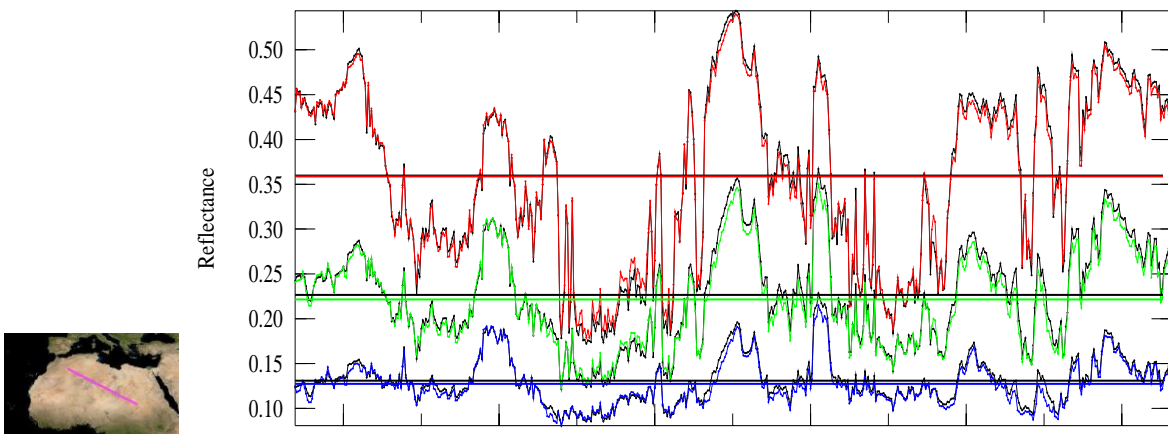


**Fig. 10.** Reflectance results for a very large transect (marked in magenta) over the Sahara for bands (0.620, 0.545, 0.459  $\mu\text{m}$ ). MCD values are in red (0.620 $\mu\text{m}$ ), green (0.545  $\mu\text{m}$ ) and blue 0.459  $\mu\text{m}$ ) and FDS values in black. The horizontal lines represent the mean values of each data sets.

Fig. 11 shows the absolute relative errors between MCD and FDS reflectances at 0.620  $\mu\text{m}$ . Clearly, there are large differences ( $> 20\%$ ) over very cloudy or snowy regions. Over snowy areas the temporal surface reconstruction depends on the snow detection algorithms, which are different in the MCD and FDS products. Over very cloudy areas, MCD results are always higher than FDS ones, these differences are mainly due to the cloudy/smoky (“milky”) pixel discrimination method. To illustrate this ‘milky pixel’ effect, an example of a 2006 average true color composite over a large area of South America is presented. **Fig. 12** is a true color composite close-up view over North of the river Amazon, in the region where the higher relative errors between MCD and FDS (see Fig. 11) are represented. The left side of **Fig. 12** illustrates that MCD reflectance values are contaminated by haze, which is not the case for the FDS products (right). **Fig. 13** is an extraction of the scene shown in **Fig. 12**, illustrating that some of the spatial fine surface structures that are visible in FDS and Google Earth images are missing in the MCD product.

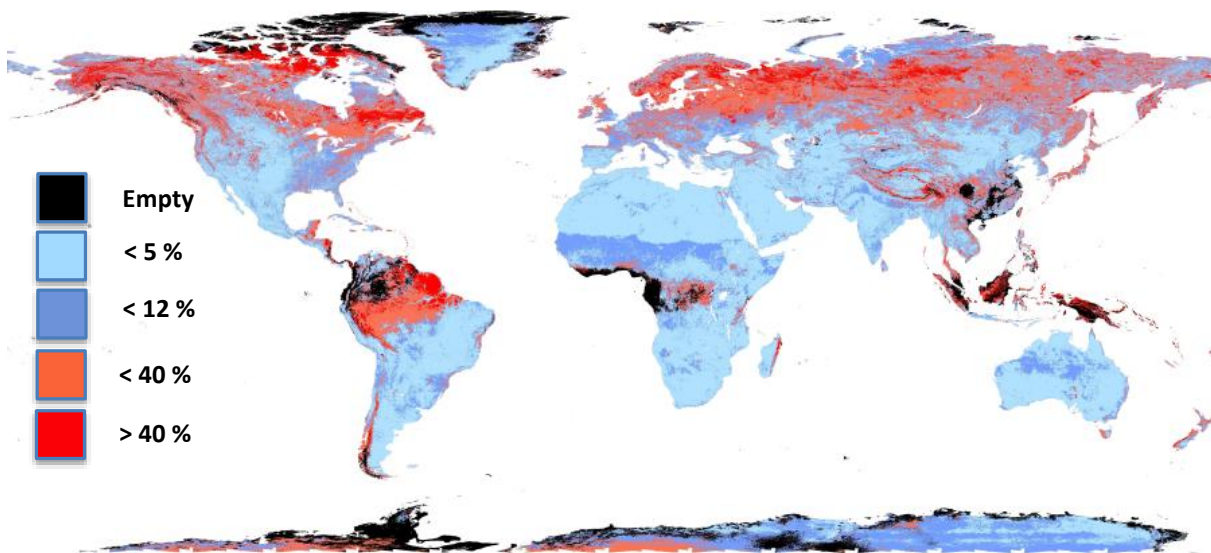
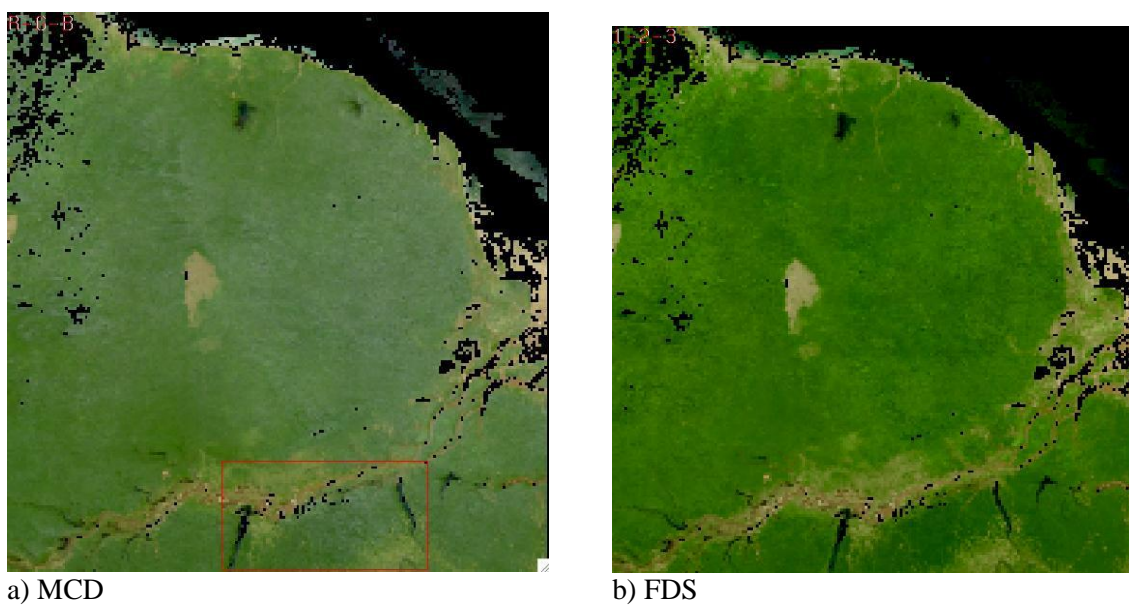


**Fig. 11.** Absolute relative errors between MCD and FDS reflectances at 0.620–0.670  $\mu\text{m}$ . Black areas labeled empty correspond to missing data in the MCD product.



a) MCD

b) FDS

**Fig. 12.** One year (2006) integration close-up views in South America north Amazon River of MCD (a) and FDS (b) reflectance synchronized values (taking only the FDS pixels whenever they exist in the MCD product).



a) MCD



b) FDS



c) Google Earth

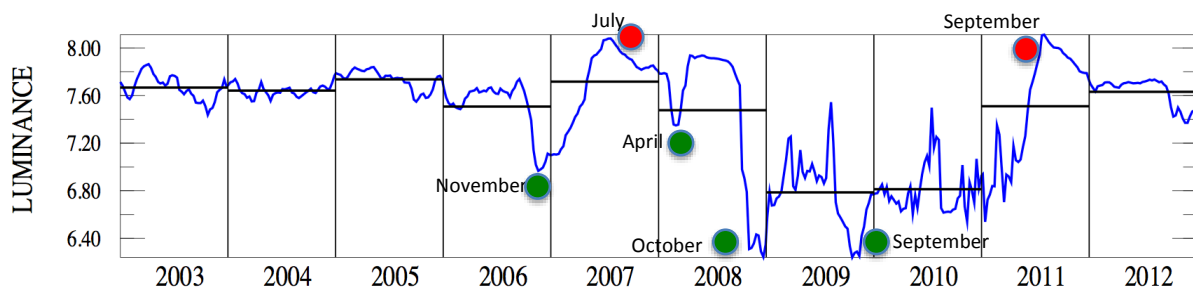
**Fig. 13.** Close-up views of the area marked in red in **Fig. 12.a**: a) MCD, b) FDS, c) Google Earth.

### 3.3 FDS V1 thematic applications.

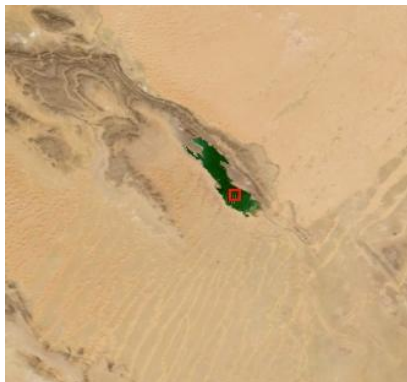
By construction, our FDS database is built from series of 8-days moving average measurement values that are clean from many artifacts present in the MODIS raw data inputs. However, the use of moving average raises the question of the capability of the database to reveal short-time surface changes. This is illustrated for three different cases: extraordinary event, natural hazard and vegetation change.

#### 3.3.1 Extraordinary event.

The Sebkhha El Melah De Kerzas (Sahara) is a well-known salt lake (Kraiem, 2012) where near mountains deposit water from time to time. Thus, on Fig. 14, the luminance of a small area within the lake (luminance giving the brightness of the visible composite image in the sRGB color space is computed as  $0.2126\text{Red}+0.7152\text{Green}+0.0722\text{Blue}$ : a low value corresponds to a dark surface, while a high value corresponds to a bright surface). The luminance magnitude follows the water cycle of the lake: when all water evaporates, a clean and very bright salt layer remains. The four years (2003-2006) temporal evolution reported in Fig. 14 highlights the drought event, after which a seasonal water level cycle is recovered.



● Salt      La Sebkhah El Mela De Kerzas  
● Water      Sahara (W1.207, N29.15)



A salted lake that receives water from the mountains. The time series makes it possible to follow the lake appearance and drying, with a strong seasonal cycle but also inter-annual variations. When the lake dries off, there is some salt at the exposed soil surface which makes it very bright.

**Fig. 14.** Luminance (representing the brightness of the visible composite image in the sRGB color space is computed as  $0.2126\text{Red} + 0.7152\text{Green} + 0.0722\text{Blue}$ ) evolution over 10 years at Sebkhah El Mela De Kerzas (Sahara).

### 3.3.2 Natural hazard.

Fig. 15 a) plots the 10-years evolution of the reflectance  $0.858 \mu\text{m}$  over a spot in a California area. The red line in the satellite image delimitates the contour of the fire extension (MODIS fire product) in August 2008. The  $0.858 \mu\text{m}$  band correlates to the seasonal vegetation variations, until it abruptly drops in August 2008, as a direct result of a huge fire. The post 2008 evolution indicates that the vegetation rapidly recovers within a few months after the fire event.

Fig. 15 b) displays the daytime Land Surface Temperature (LST) and the luminance of a huge area located in the north west of Argentina. The luminance follows annual variations with the exception of the two dark peaks in 2007 and 2009, which are correlated to huge floods of the Rio Paraná.

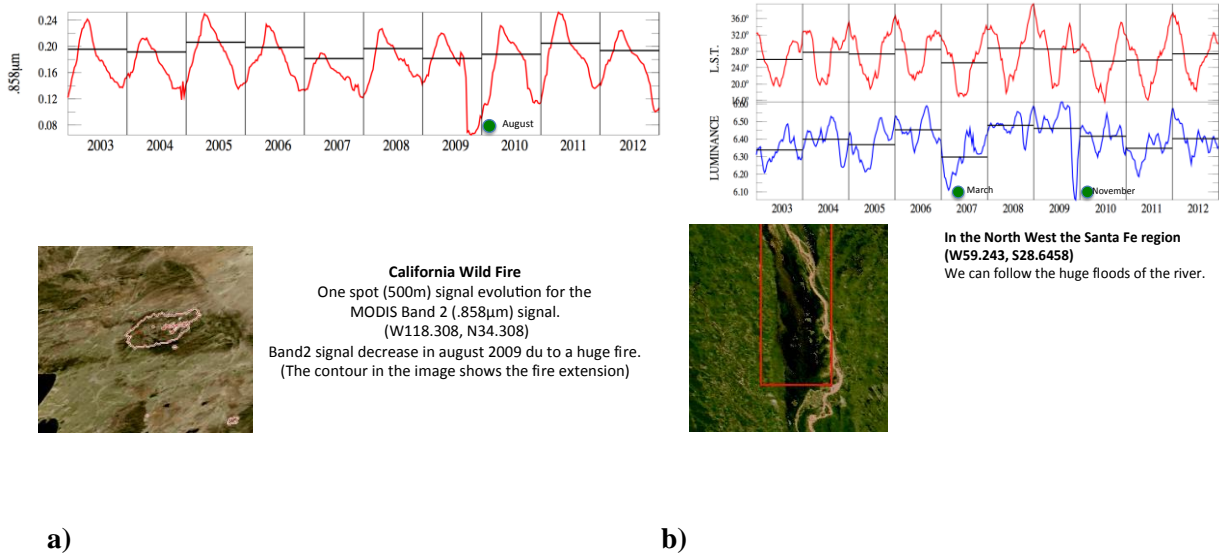


**Fig. 15.** a) 10-years evolution of the 0.858 μm reflectance over a spot in a California area. The red line in the satellite image shows the contour of the August 2008 fire extension (MODIS fire product); b) 10-years evolution of the luminance and land surface temperature (LST) in North West Argentina revealing huge floods of the Rio Paraná.

### 3.3.3 Vegetation change.

As an illustration of the capability of FDS V1 to monitor vegetation changes, Fig. 16 reports NDVI time plots in two very different areas, namely a dry spot in Sahel, with extremely short vegetation peaks, and the intensively cultivated Nile Delta, where several harvests happen every year.

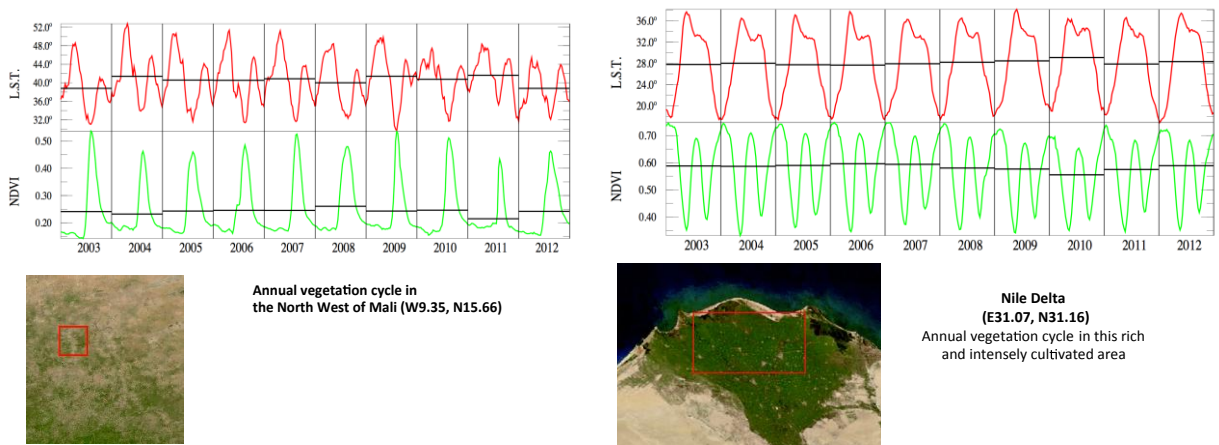


**Fig. 16.** 10-years NDVI and Land Surface Temperature (LST) in two very distinct areas: a) short peaks of vegetation on the Sahel; b) the intensively cultivated Nile Delta.

## 4 Conclusion

A new and improved land surface reflectance database, named FondsDeSol is presented using 10-years MODIS acquisitions onboard Terra and Aqua platforms. The main improvements with respect to the MODIS products such as MCD43C4 are two-fold: 1) a better cloud filtering minimizing the “milky pixel effect” and 2) a temporal interpolation for screened pixels during an entire 8 days period to correct very cloudy regions. The validation tests show that most artifacts inherent to the input MODIS data have been well eliminated. All the presented temporal series demonstrate the capability of FDS V1 database to monitor seasonal

evolutions. This indicates that the reflectance reconstruction process yields reflectance values over the whole Earth surfaces that are reasonable and approaching realistic observations.

The benefit of using such database is illustrated in 3 cases: extraordinary events, natural hazards and vegetation changes. They highlight the potential of the V1 FDS to reveal Earth surface evolutions.

However, in its nominal version, the FDS database suffers from two limitations. The first one is its size of several terabytes. The second limitation is related to the fact that the spectral reflectances are so far only computed for the MODIS bands. Statistical estimation methods can be applied to extend the spectra reflectances to the entire optical domain (ADAM-ESA).

It is noteworthy, that the underlying algorithm of FDS V1 has been implemented in two collaborative projects. The spatial sampling and the spectral extensions approaches have been used in the European ESA-ADAM project (ADAM-ESA) to create a reference FDS database at 10 km with a monthly sampling over year 2005. Within the French ECLIPS project (ANR-11-ASTR-0042), the FDS database will be integrated in a near future the 3D radiative transfer code MATISSE (Simoneau et al., 2009) to support the design of future remote sensing sensors.

### **Acknowledgments**

Christine Deroo (LOA), developer of the FDS website ([http://newtec.univ-lille1.fr/fondsdesol/index\\_ch.html](http://newtec.univ-lille1.fr/fondsdesol/index_ch.html)) is gratefully acknowledged. This study was funded by both ESA (ADAM project) and the French National Agency for Research under the contract ANR-11-ASTR-0042. All MODIS products are courtesy of the online Data Pool at the NASA Land Processes Distributed Active Archive Center (LP DAAC), USGS/Earth Resources Observation and Science (EROS) Center, Sioux Falls, South Dakota.

## References

- ADAM-ESA. The ADAM products have been collected from the ADAM database ([adam.noveltis.com](http://adam.noveltis.com)), and were produced by the ADAM team under the European Space Agency (ESA) study contract Nr C4000102979.
- Arino, O.P., Bicheron F., Achard J., Latham R.W., and Weber J.L. (2008). "GLOBCOVER the Most Detailed Portrait of Earth." *ESA Bulletin-European Space Agency* 136: 24–31.
- Bacour C., Bréon F.-M. (2005), Variability of biome reflectance directional signatures as seen by POLDER, *Remote Sensing of the Environment*, 98: 80-95.
- Baldrige, A. M., Hook S.J., Grove C.I. and Rivera, G. (2009). The ASTER Spectral Library Version 2.0. *Remote Sensing of Environment*, vol 113, pp. 711-715.
- Börner A., Wiest L., Keller P., Reulke R., Richter R., Schaepman M., and Schläpfer D. (2001). "SENSOR: A tool for the simulation of hyperspectral remote sensing systems," *ISPRS J. Photogramm. Remote Sens.*, vol. 55, pp. 299–312
- Bartholomé E., and Belward A. S. (2005). "GLC2000: A New Approach to Global Land Cover Mapping from Earth Observation Data." *International Journal of Remote Sensing* 26: 1959–77.
- Bicheron P., Defourny P., Brockmann C., Schouten L., Vancutsem C., Huc M., Bontemps S., Leroy M., Achard F., Herold M., Ranera F., Arino O. (2008). GLOBCOVER: Products Description and Validation Report. ESA Report.
- Bontemps S., Defourny P., Van Bogaert E., and Arino O. (2010). GLOBCOVER2009 ProductsDescription and Validation Report. Accessed January 20, 2012. [https://globcover.s3.amazonaws.com/LandCover2009/GLOBCOVER2009\\_Validation\\_Report\\_1.0.pdf](https://globcover.s3.amazonaws.com/LandCover2009/GLOBCOVER2009_Validation_Report_1.0.pdf).
- Carrere V., Briottet X., Jacquemoud S., Marion R., Bourguignon A., Chami M., Chanussot J., Chevrel S., Deliot P., Dumont M., Foucher P.-Y., Minghelli-Roman A., Sheeren D., Weber C., Lefevre-Fonollosa M.-J., Manda M., The French EO high spatial resolution hyperspectral dual mission HYPXIM – An update, *IGARSS 2014 / 35th Canadian Symposium on Remote Sensing*.
- Cota S. A., Bell R. H. B. J. T., Dutton T. E., Florio C. J., Franz G. A., Grycewicz T. J., Kalman L. S., Keller R. A., Lomheim T. S., Paulson D. B., and Wilkinson T. S. (2010). PICASSO: An end-to-end image simulation tool for space and airborne imaging systems *J. Appl. Remote Sens.*, vol. 4, pp. 1–36.
- Fauqueux S., L. Labarre, K. Caillault, C. Malherbe, A. Roblin, B. Rosier, P Simoneau, MATISSE-v2.0, a radiative transfer code for advanced infrared Earth modeling, *OPTRO 2012*
- Friedl, M. A., Mciver D. K., Hodges J. C. F., Zhang X. Y., Muchoney D., Strahler A. H., Woodcock C. E., Gopal S., Schneider A., Cooper A., Baccini A., Gao F., and Schaaf C.. (2002). "Global Land Cover Mapping from MODIS: Algorithms and Early Results." *Remote Sensing of Environment* 83: 287–302.
- Friedl, M. A., Sulla-Menashe D., Tan B., Schneider A., Ramankutty N., Sibley A., and Huang X. M. (2010). MODIS Collection 5 Global Land Cover: Algorithm Refinements and Characterization of New Datasets. *Remote Sensing of Environment* 114: 168–82.
- Friedl M.A., McIver D.K., Zhang X.Y., Hodges J.C.F., Schnieder A., Bacinni A., Strahler A.H., Cooper A., Gao F., Schaaf C., Liu W. (2001), Global land cover classification results from MODIS; *Geoscience and Remote Sensing Symposium*, 2001. *IGARSS apos; 01. IEEE 2001 International*, 2, 733 - 735 (DOI: 10.1109/IGARSS.2001.976618).
- Gong P., Wang J., Yu L., Zhao Y., Zhao Y., Liang L., Niu Z., Huang X., Fu H., Liu S., Li C., Li X., Fu W., Liu C., Xu Y., Wang X., Cheng Q., Hu L., Yao W., Zhang H., Zhu P., Zhao Z., Zhang H., Zheng Y., Ji L.,

- Zhang Y., Chen H., Yan A., Guo J., Yu L., Wang L., Liu X., Shi T., Zhu M., Chen Y., Yang G., Tang P., Xu B., Giri C., Clinton N., Zhu Z., Chen J. & Chen J. (2013). Finer resolution observation and monitoring of global land cover: first mapping results with Landsat TM and ETM+ data, *International Journal of Remote Sensing*, 34, 2607-2654.
- Gonzalez, L., Bréon, F.M., Briottet, X., (2010) Construction of a Global Database of Surface Reflectance and Emissivity at a Sub km Resolution, *PIERS* 6, 195
- Hall, D. K., Salomonson V. V., and Riggs G. A. (2006). MODIS/Terra Snow Cover 8-Day L3 Global 500m Grid. Version 5. Boulder, Colorado USA: National Snow and Ice Data Center.
- Hosgood, B., Jacquemoud S., Andreoli G., Verdebout J., Pedrini G. and G. Schmuck. Leaf Optical Properties EXperiment 93 (LOPEX93), Report EUR-16095-EN, European Commission, Joint Research Centre, Institute for Remote Sensing Applications, Ispra, Italy (1995).
- Itten K. I., Schaepman M., Vos L. D., Hermans L., Schläpfer D., and Droz F., APEX—Airborne PRISM experiment: A new concept for an airborne imaging spectrometer, in Proc. 3rd Int. Airborne Remote Sensing Conf. Exhibition, Copenhagen, Denmark, 1997, pp. 181–188.
- Kokhanovsky, A. A., Zege, E. P. (2004a) Scattering optics of snow, *Applied Optics*, 43, 1589-1602.
- Kokhanovsky A.A., Zege E.P., Scattering optics of snow; *Appl. Opt.* 43, issue 7, 1589-1602, 1 March 2004b
- Kokhanovsky A. A., Bréon F.-M. (2012) Validation of an analytical snow BRDF model using PARASOL multi-angular and multispectral observations, *IEEE Geosci. Rem. Sens. Letters*, 9, 928-932.
- Kraiem, H, Biophysical and socio-economic impacts of climate changes on wetlands in the Mediterranean, Mediterranean Regional Roundtable Athens, Greece. December 10-11, 2002
- Lagouarde J.-P., Bach M., Sobrino, J., Boulet, G., Briottet, X., Cherchali S., Coudert, B., Dadou, I., Dedieu, G., Gamet, P., Hagolle, O., Jacob, F., Nerry, F., Olivoso, A., Otle, C., Roujean J.-L., Fargant, G. (2013) The MISTIGRI Thermal Infrared project: scientific objectives and mission specifications, *International Journal of Remote Sensing*, iFirst, 1–30, <http://dx.doi.org/10.1080/01431161.2012.716921>
- Lewis P., Guanter L., Lopez Saldana G., Muller J.-P., Watson G., Shane N., Kennedy T., Fisher J., Domenech C., Preusker R., North P., Heckel A., Danne O., Kraämer U., Zühlke M., Fomferra N., Brockmann C. Crystal Schaaf The ESA GlobAlbedo Product, Proc. IGARSS 2012.
- Maignan, F., Bréon, F.-M., Lacaze, R. (2004a). Bidirectional reflectance of Earth targets: Evaluation of analytical models using a large set of space-borne measurements with emphasis on the Hot Spot. *Remote sensing of Environment*, vol. 90 pp. 210-220.
- Maignan, F., Bréon, F.M., Lacaze, R., (2004b) Bidirectional reflectance of Earth targets: Analytical modeling and validation against a large data set of satellite observations.;; *Rem. Sens. Env.*, 90, 210-220.
- Meygret A., Dinguirard M., Henry P., Poutier L., Lafont S., Hazane P. (1997), The SPOT Histogram Data Base, *SPIE*. 2957, 322-330.
- Miesch C., Briottet X., Kerr Y. H. (2004) Phenomenological analysis of simulated signals observed over shaded areas in a urban scene », *IEEE Transactions on Geoscience and Remote Sensing*, 42, 434-442.
- Miesch C., Poutier L., Achard V., Briottet X., Lenot X., Boucher Y. (2005). Direct and Inverse Radiative Transfer Solutions for Visible and Near-Infrared Hyperspectral Imagery. *IEEE TGARS*, 43, 1552-1562.
- Land Processes Distributed Active Archive Center (LP DAAC), 2006, MDC43C4. NASA EOSDIS Land Processes DAAC, USGS Earth Resources Observation and Science (EROS) Center, Sioux Falls, South

- Dakota (<https://lpdaac.usgs.gov>), accessed September 5, 2015, at [https://lpdaac.usgs.gov/dataset\\_discovery/modis/modis\\_products\\_table/mcd43c4](https://lpdaac.usgs.gov/dataset_discovery/modis/modis_products_table/mcd43c4).
- Land Processes Distributed Active Archive Center (LP DAAC), 2000, MOD12Q1. NASA EOSDIS Land Processes DAAC, USGS Earth Resources Observation and Science (EROS) Center, Sioux Falls, South Dakota (<https://lpdaac.usgs.gov>), accessed September 5, 2015, at [https://lpdaac.usgs.gov/dataset\\_discovery/modis/modis\\_products\\_table/mcd12q1](https://lpdaac.usgs.gov/dataset_discovery/modis/modis_products_table/mcd12q1)
- Land Processes Distributed Active Archive Center (LP DAAC), 2000, MOD09A1. NASA EOSDIS Land Processes DAAC, USGS Earth Resources Observation and Science (EROS) Center, Sioux Falls, South Dakota (<https://lpdaac.usgs.gov>), accessed September 5, 2015, at [https://lpdaac.usgs.gov/products/modis\\_products\\_table/mod09a1](https://lpdaac.usgs.gov/products/modis_products_table/mod09a1).
- Land Processes Distributed Active Archive Center (LP DAAC), 2000, MOD11. NASA EOSDIS Land Processes DAAC, USGS Earth Resources Observation and Science (EROS) Center, Sioux Falls, South Dakota (<https://lpdaac.usgs.gov>), accessed September 5, 2015, at [http://modis.gsfc.nasa.gov/data/dataproduct/dataproducts.php?MOD\\_NUMBER=11](http://modis.gsfc.nasa.gov/data/dataproduct/dataproducts.php?MOD_NUMBER=11)
- Land Processes Distributed Active Archive Center (LP DAAC), 2000, MOD12. NASA EOSDIS Land Processes DAAC, USGS Earth Resources Observation and Science (EROS) Center, Sioux Falls, South Dakota (<https://lpdaac.usgs.gov>), accessed September 5, 2015, at [http://modis.gsfc.nasa.gov/data/dataproduct/dataproducts.php?MOD\\_NUMBER=12](http://modis.gsfc.nasa.gov/data/dataproduct/dataproducts.php?MOD_NUMBER=12).
- Muller J.-P., López G., Watson G., Shane N., Kennedy T., Yuen P., Lewis P., Fischer J., Guanter L., Domench C., Preusker R., North P., Heckel A., Danne O., Krämer U., Zühlke M., Brockmann C., Pinnock S. (2012), The ESA GlobAlbedo Project for mapping the Earth's land surface albedo for 15 Years from European Sensors., paper presented at IEEE Geoscience and Remote Sensing Symposium (IGARSS) 2012, IEEE, Munich, Germany, 22-27.7.12.
- Muller J.-P., López G., Watson G., Shane N., Kennedy T., Yuen P., Lewis P., Fischer J., Guanter L., Domench C., Preusker R., North P., Heckel A., Danne O., Krämer U., Zühlke M., Brockmann C., Pinnock S. (2011), The ESA GlobAlbedo Project for mapping the Earth's land surface albedo for 15 Years from European Sensors., paper presented at the European Geophysical Union conference, Geophysical Research Abstracts, Vol. 13, EGU2011-10969
- Parente M., Clark J. T., Brown A. J., and Bishop J.L. (2010). End-to-end simulation and analytical model of remote-sensing systems: Application to CRISM. *IEEE Trans. Geosci. Remote Sens.*, 48, 3877–3054.
- Rousset-Rouviere L., Coudrain C., Fabre S., Baarstad I., Fridman A., Løke T., Blaaberg S., Skauli T., Sysiphe, an airborne hyperspectral imaging system for the VNIR-SWIR-MWIR-LWIR region, 7th EARSeL Workshop on Imaging Spectroscopy Edinburgh, Scotland, 11th – 13th April, 2011
- Segl K., Guanter L., Rogass C., Kuester T., Roessner S., Kaufmann H., Sang B., Mogulsky V., and Hofer S. (2012). EeteS—The EnMAP End-to-End Simulation Tool, *IEEE Journal of Selected Topics in Applied Earth Observations and Remote Sensing*, 5, 522 – 530.
- Simoneau P., Caillault K., Malherbe C., Labarre L., Huet T., Fauqueux S., and Rosier, B. (2009): MATISSE-v1.5 and MATISSE-v2.0: new developments and comparison with MIRAMER measurements. *Proc. SPIE*, Vol. 7300, 73000L.
- Tateishi, R., Uriyangqai B., Al-Bilbisi H., Ghar M. A., Tsend-Ayush J., Kobayashi T., Kasimu A., Thanh H. N., Shalaby A., Alsaaidh B., Enkhzaya T., Tana G., and Sato H. P. (2011). Production of Global Land Cover, GLCNMO. *International Journal of Digital Earth* 4, 22–49.
- Verhoef W. and Bach H. (2003). Simulation of hyperspectral and directional radiance images using coupled biophysical and atmospheric radiative transfer models. *Remote Sens. Environ.*, 87, 23–41.